Cancer Therapy

DOI: 10.1002/anie.201408472

Marriage of Scintillator and Semiconductor for Synchronous Radiotherapy and Deep Photodynamic Therapy with Diminished Oxygen Dependence**

Chen Zhang, Kuaile Zhao, Wenbo Bu, Dalong Ni, Yanyan Liu, Jingwei Feng, and Jianlin Shi**

Abstract: *Strong oxygen dependence and limited penetration depth are the two major challenges facing the clinical application of photodynamic therapy (PDT). In contrast, ionizing radiation is too penetrative and often leads to inefficient radiotherapy (RT) in the clinic because of the lack of effective energy accumulation in the tumor region. Inspired by the complementary advantages of PDT and RT, we present herein the integration of a scintillator and a semiconductor as an ionizing-radiation-induced PDT agent, achieving synchronous radiotherapy and depth-insensitive PDT with diminished oxygen dependence. In the core–shell Ce^{III}-doped $LiYF_4@SiO_2@ZnO$ structure, the downconverted ultraviolet fluorescence from the Ce^{III}-doped $LiYF_4$ nanoscintillator under ionizing irradiation enables the generation of electron–hole (e^-–h^+) pairs in ZnO nanoparticles, giving rise to the formation of biotoxic hydroxyl radicals. This process is analogous to a type I PDT process for enhanced antitumor therapeutic efficacy.*

As an emerging noninvasive treatment for carcinoma, photodynamic therapy (PDT) has received considerable attention in recent years. PDT employs light-excited photosensitizers to activate the transformation of surrounding triplet oxygen ($^3O_2$) into cytotoxic singlet oxygen ($^1O_2$), in most cases through a type II pathway using O_2 as the $^1O_2$ source, and to cause irreversible damage to malignant cells.[1] However, a number of intractable problems have greatly hindered its practical application in the clinic. As a result of a general type II mechanism for most photosensitizers, conventional PDT typically involves significant O_2 consumption[2] and is therefore strongly oxygen-tension sensitive. This sensitivity leads to drastically decreased antitumor therapeutic efficacy during continuing treatment, especially for the inherent hypoxic tumor tissue,[2,3] which is considered as a major obstacle for most cancer therapies.[4] Furthermore, the effective excitation wavelength of most photosensitizers is located in the ultraviolet or visible-light regions, which suffers from greatly limited penetration depth in human tissues.[1a,5] Despite some efforts to develop near-infrared-induced PDT by employing some special photosensitizers and upconversion materials,[6] these still fail to make satisfactory progress against deep-seated cancers. Therefore, clinical medicine urgently awaits the development of oxygen-insensitive and depth-independent PDT for cancer therapy.

In comparison, radiotherapy (RT), a conventional commonly applied treatment modality which employs ionizing radiation to control or kill malignant cells, is virtually immune from the restriction of penetration depth. When considering the complementary advantages of both RT and PDT, we wondered if it would be possible to utilize ionizing radiation to induce localized PDT with diminished oxygen dependence. However, to achieve this, several significant obstacles need to be overcome. First, the clinical high-energy radiation (X-ray and gamma ray) for cancer treatment, whose photon energy is in the range of several kiloelectronvolt (keV) to several megaelectronvolt (MeV), is incapable of effectively activating traditional photosensitizers with a singlet–triplet energy gap of several electronvolt (typically 1–3 eV).[5] Recently, a new X-ray-activated complex and a novel system composed of X-ray-excited afterglow nanoparticles and photosensitizer have been proposed in pilot studies by Chen et al.,[7] which may provide a solution to bridge the wide energy mismatch. Second, although a recent physical study has demonstrated the generation of singlet oxygen using a nanohybrid of Tb_2O_3 and porphyrin under X-ray irradiation,[8] most organic photosensitizers may suffer from serious photodestruction during ionizing irradiation, losing their photodynamic effectiveness.[9] Third, hypoxic tumor cells are known to be highly resistant to radiotherapy.[10] Thus, it is necessary to find a fundamental approach to urgently overcome the common inherent shortcomings to RT and PDT by diminishing the oxygen tension dependency.

Herein, we report a novel strategy in which ionizing radiation is applied to induce deep PDT with diminished oxygen dependence. A nanosized scintillator was used as a connecting bridge between the energy levels of the radiation

[*] Dr. C. Zhang, Prof. W. Bu, Dr. D. Ni, Dr. Y. Liu, Prof. J. Feng, Prof. J. Shi
State Key Laboratory of High Performance Ceramics and Superfine Microstructure, Shanghai Institute of Ceramics
Chinese Academy of Sciences
1295 Ding-xi Road, Shanghai 200050 (P.R. China)
E-mail: wbbu@mail.sic.ac.cn
jlshi@mail.sic.ac.cn
Prof. K. Zhao
Department of Radiology, Shanghai Cancer Hospital
Fudan University, 270 Dong-an Road, Shanghai 200032 (P.R. China)

[**] This work has been financially supported by the National Natural Science Foundation of China (Grant No. 51372260, 51132009, 21172043), the Shanghai Rising-Star Program (Grant No. 12QH1402500). We thank Shiming Huang and Fengrui Li from the School of Physics Science and Engineering, Tongji University, for assistance with the X-ray induced emission spectroscopy measurements. Thanks to Linlin Zhang, Heliang Yao, Qingfeng Xiao, Huaiyong Xing, Wenpei Fan, and Jianan Liu from the Shanghai Institute of Ceramics, Chinese Academy of Sciences, for useful discussions.

Supporting information for this article is available on the WWW under http://dx.doi.org/10.1002/anie.201408472.

source and the bandgap of the photosensitizers. The scintillator has the distinctive property that high-energy electromagnetic radiation can be downconverted giving rise to luminescence in the UV/visible region of the spectrum. Additionally, the photodestruction could be largely prevented by the employment of highly photostable inorganic semiconductors instead of organic photosensitizers. Aiming at the beneficial combination of a nanoscintillator and a semiconductor (Figure 1 a), octahedral Ce^{III}-doped $LiYF_4$ scintillating

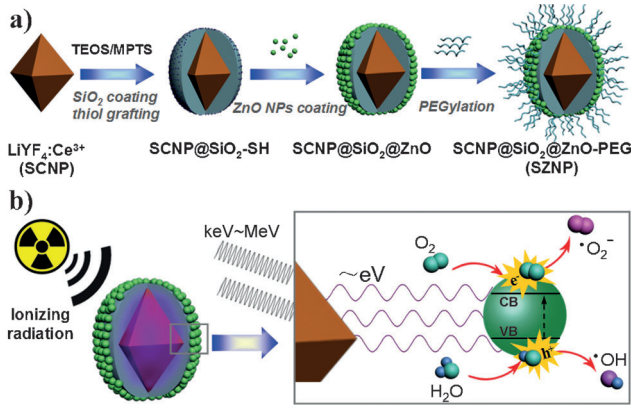

Figure 1. a) Schematic illustration of the synthetic route to monodisperse SZNPs and b) the mechanism of ionizing radiation-induced photodynamic therapy. The electron–hole (e^-–h^+) pair is formed after exposure to ionizing radiation. TEOS = tetraethyl orthosilicate. MPTS = (3-mercaptopropyl) trimethoxysilane.

nanoparticles (SCNP; see Figure S1 a in the Supporting Information) were first prepared as a nanoconverter, whose bulk crystal shows an unusual ultraviolet emission with high luminescence efficiency under high-energy radiation.[11] After coating with SiO_2 (Figure S1 b) and incorporation of thiol groups, ultrafine ZnO semiconductor nanoparticles (Figure S1 c) were attached firmly to the surface of $SCNP@SiO_2$ nanoparticles by strong metal–sulfur bonds. Further surface modification with PEG (poly(ethylene glycol)) to form $SCNP@SiO_2@ZnO$-PEG nanoparticles (denoted SZNP) further enhanced biological compatibility (Figure S1 d). Figure 1 b gives the mechanism of the ionizing-radiation-induced PDT. In brief, the SCNP seed is excited using ionizing radiation and emits numerous photons of low energy that match the bandgap of surface-bound ZnO nanoparticles. The subsequent excitons formed (the electron–hole (e^-–h^+) pairs) interact with water and oxygen molecules to form free radicals.[12] Notably, similar to type I PDT, the highly reactive hydroxyl radicals (•OH) are derived from the reaction between the hole (h^+) and the absorbed water instead of O_2,[13] which essentially minimizes the oxygen-tension dependency for the generation of reactive oxygen species.[2,14] Furthermore, considering the inherent antitumor efficacy of ionizing radiation, this new method employing synchronous radiotherapy and PDT with a single excitation source would be of great clinical interest.

As depicted in Figure 2 and Figure S1 d, the transmission electron microscopic (TEM) images show a high uniformity and a sharp (well-defined) particle size distribution of the approximately spherical SZNPs with an average diameter of 33.8 nm. Additionally, apparent contrast differences in high-magnification TEM images and scanning TEM (STEM) images provide direct evidence for the formation of a well-defined Ce^{III}-doped $LiYF_4$ core@SiO_2@ZnO structure for the SZNP, whose chemical composition was further confirmed through corresponding element mapping (Figure 2 g). Additionally, the excellent stability of the SZNPs against radiation and their longstanding monodispersity (Figure S2) are due to the firm coating of the well-crystallized ZnO nanoparticles and the successful final PEGylation reaction (Figure S1).

The X-ray-induced emission spectrum of the SCNPs exhibit strong emission bands at $\lambda = 305$ and 325 nm (Figure 3 a), which can be traced to the transitions from the lowest level of the 5d configuration in the Ce^{III} ion to the $^2F_{5/2}$ and $^2F_{7/2}$ levels, respectively, of the $4f^1$ configuration (Figure 3 a, inset). Importantly, the emission derived from the inner SCNPs corresponds perfectly with the absorption of the ZnO nanoparticles (Figure 3 a), ensuring that effective energy transfer can occur between the SCNPs and the ZnO nanoparticles. This energy match is further confirmed by the fact that the fluorescence of the SZNPs is fully quenched under X-ray irradiation, excluding the possibility that the SiO_2 interlayer could act as a potential light absorber, as evidenced by the well-maintained emission of the $SCNP@SiO_2$ nanoparticles.

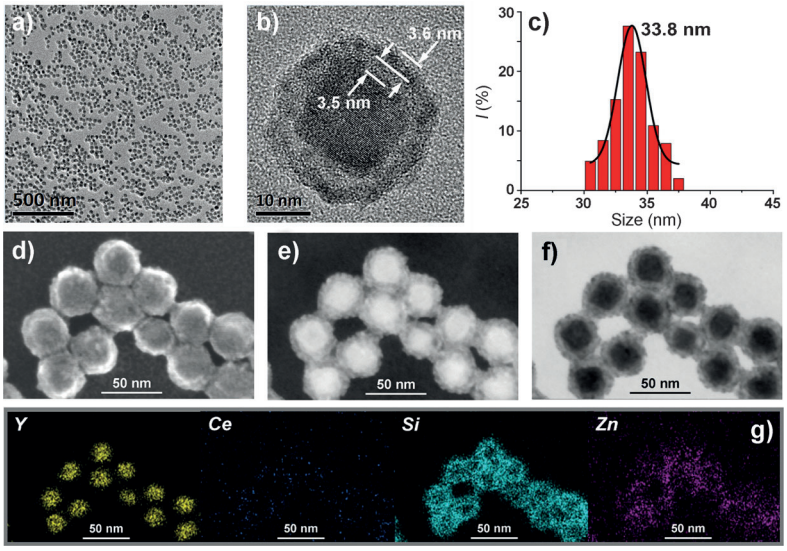

Figure 2. Structural and compositional characterization of SZNPs. TEM images at a) low (scale bar = 500 nm) and b) high (scale bar = 10 nm) magnifications and c) the corresponding size distribution of SZNPs. STEM image of SZNPs using d) SEM, e) dark-field, and f) bright-field modes. h) Corresponding element mappings (for Y, Ce, Si, and Zn) of SZNPs. Scale bars in (d–g) = 50 nm.

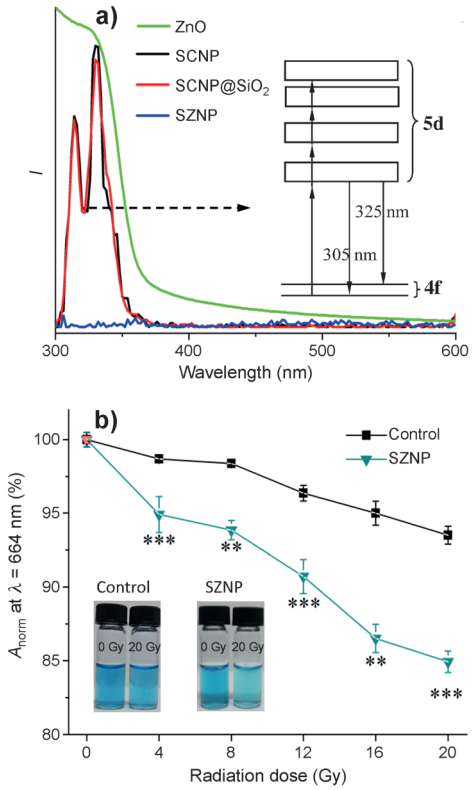

Figure 3. The investigation of SZNPs as an agent for ionizing-radiation-induced PDT. a) Plot showing the emission spectra of SCNPs (black), SCNP@SiO_2 nanoparticles (red), and SZNPs (blue) under X-ray excitation and the UV/Vis absorption spectrum of ZnO nanoparticles (green). Inset in (a): the energy-level diagram of Ce^{III} in a $LiYF_4$ nanocrystal. b) Comparison of ROS production between the control group and the group treated with SZNPs under varied radiation doses as determined by the decay of MB absorption at $\lambda = 664$ nm. Experiments were performed in triplicate. Data are expressed as mean ± standard errors ($n = 3$). Statistical analysis was performed using the Student's two-tailed t test (**$P < 0.01$ and ***$P < 0.001$). Inset in (b): photographs of each group before and after 20 Gy irradiation.

By using a colorimetric method based on bleaching of methylene blue (MB) after selective ·OH trapping,[15] we compared the ROS (·OH) yield of the SZNPs in water to a control experiment without SZNPs under varied radiation doses (Figure 3b). As a result of the ionizing radiation, the free radicals formed by radiolysis cause a gradual decay of MB absorption in the control experiment.[16] Remarkably, the introduction of SZNPs further intensify this process with a considerably increased decay rate of MB absorption, implying the critical role of the SZNPs in promoting ROS generation under X-ray irradiation. The notably increased type I PDT related ·OH production from the reaction of the absorbed water with the photogenerated holes in ZnO nanoparticles[13] indicates a minimized oxygen dependence of the ROS yield. This minimized dependence is because of the participation of water as the ROS source, replacing O_2 in the type II pathway.[2] Additionally, the efficiency of this ROS-generation process is calculated to be about 3.4% (details in the Supporting Information), which benefits from a negligible heat effect (Figure S3) and the weak luminescence of the SZNPs under X-ray irradiation (Figure 3a and Figure S4). These proof-of-principle experiments qualify the SZNPs as an efficient ROS producer with diminished oxygen dependence under ionizing radiation.

We next evaluated the ability of the as-synthesized SZNPs to generate ROS in live cells after exposure to X-ray radiation. ROS generation was examined by using the non-fluorescent molecule 2′,7′-dichlorofluorescein diacetate (DCFH-DA), which can be oxidized to the fluorescent DCF by ROS. Contrastive measurements of fluorescence levels were performed simultaneously in normoxic (21% O_2) and hypoxic (2% O_2) HeLa cells. As shown in Figure 4a and 4b, only a negligible fluorescence increase can be detected for the group treated with SZNPs alone compared to the control group without SZNPs, which demonstrates that SZNPs are a safe biological agent with no significant influence on intracellular ROS generation. After exposure to X-ray radiation (3 Gy), the normoxic cells show a 1.5-fold enhancement in DCF fluorescence intensity, whereas that of hypoxic cells remains at the control level. The increased ROS caused by exposure of the cells to the radiation may be attributed to the radiolysis of ionizing radiation, whose generation depends highly on the ambient oxygen tension.[17] In comparison, ROS production can be significantly promoted in cells exposed to radiation and treated with SZNPs in both normoxia and hypoxia cases. The almost comparable enhancement in the generation of ROS indicates that the SZNP-based PDT under ionizing radiation is of negligible oxygen-tension dependence.

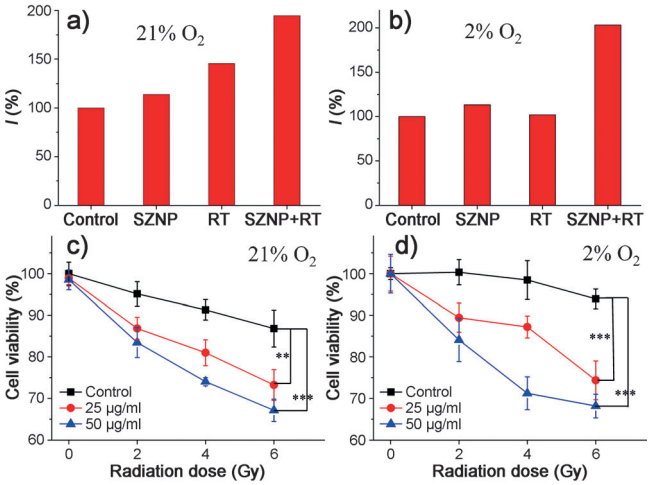

Figure 4. In vitro administration to HeLa cells of ionizing-radiation-induced synchronous radiotherapy and PDT based on the as-synthesized SZNPs. Relative intensities of ROS-induced DCF fluorescence measured from flow cytometry analyses after incubation of the cells with SZNPs (50 μg mL^{-1}) in a) normoxic (21% O_2) and b) hypoxic (2% O_2) HeLa cells. In (a) and (b), control and SZNP indicate cells not exposed to radiation. RT and SZNP + RT denote control and SZNP-incubated HeLa cells, respectively, which have been exposed to X-ray irradiation (3 Gy). Viabilities of c) normoxic and d) hypoxic HeLa cells treated with 25 μg mL^{-1} and 50 μg mL^{-1} SZNPs for 24 h followed by varied doses of X-ray radiation (0, 2, 4, and 6 Gy). Values are in mean ± standard errors ($n = 8$). Statistical analysis was performed using the Student's two-tailed t test (**$P < 0.01$ and ***$P < 0.001$).

The flow cytometry results were further confirmed from the confocal images of ROS-generated DCF fluorescence in the cells (Figure S5).

Having established SZNPs as an efficient intracellular ROS producer with low cytotoxicity (Figure S6), cell activity was investigated upon incubation of cells with different concentrations of SZNPs. In contrast to the control, significant reductions in the cell viabilities of groups treated with SZNPs can be detected under X-ray irradiation for both normoxic and hypoxic HeLa cells, which shows a positive correlation with the radiation dose and amount of the SZNPs employed (Figure 4c and 4d). Notably, consistent with the results of the ROS yield experiments, the hypoxic cell viability changes little under X-ray irradiation alone (i.e. without SZNP incubation), in contrast to that of normoxic cells. This difference implies that the hypoxic cells are much more resistant to the ionizing radiation than those with normal levels of oxygen.[18] The result can be verified by an apoptosis assay based on flow cytometry (Figure S7), which further confirms the essential influence of oxygen level in radiotherapy for the generation of ROS (Figure 4b and Figure S5). However, the oxygen tension shows much less influence on cell death under X-ray irradiation in the presence of SZNPs. The significantly increased ratio of the late apoptotic cells (G2 region in Figure S7) confirms the highly efficient SZNP-mediated PDT (both in normoxic and hypoxic cells). The efficiency of the process is because of the irreversible oxidative damage of DNA, lipids, and proteins by water-generated hydroxyl radicals analogous to type I PDT, which is much more reactive than the singlet oxygen.[19]

Encouraged by the remarkable efficacy of PDT in vitro and the confirmed excellent in vivo biocompatibility (see the Supporting Information), we performed preliminary radiation therapy to confirm the potential of the SZNPs as an efficient agent in ionizing-radiation-induced PDT in vivo. Excitingly, the tumor treated with SZNPs and exposed to X-ray radiation of 8 Gy (denoted by RT) were almost completely inhibited after 15 days in comparison to a just slight reduction in tumor growth rate for radiotherapy alone (Figure 5a). The pathological tumor-tissue sections obtained 48 hours after treatment were used to further evaluate the treatment efficacy in vivo. Corresponding to the tumor growth curve, no detectable damage can be found in hematoxylin and eosin (H&E) stained tumor sections which have not been exposed to X-ray irradiation (Figure 5b,c). The fact that the tumor tissue remains intact and undamaged indicates the negligible in vivo toxicity of SZNPs. It is notable that the tumor tissue (Figure 5d) is clearly damaged after radiotherapy alone, and such obvious damage with a decreased intensity of tumor tissue becomes more significant when the tissue is treated with both SZNPs and X-ray irradiation (Figure 5e). As shown in the magnified images in Figure 5f, only slight swelling of the nuclei in the tumor tissue treated with just X-ray radiation is observed. In contrast, prominent late-stage apoptosis featuring karyopyknosis, karyorrhexis, and significant formation of apoptotic bodies is observed in the tumor tissue treated with SZNP plus radiation (Figure 5g), representing the combined effect of radiotherapy and SZNP-assisted PDT. These preliminary results undoubtedly qualify SZNPs as a potential ionizing-radiation-induced PDT agent.

In summary, herein we report a novel strategy for synchronous radiotherapy and ionizing-radiation-induced deep PDT. This method demonstrates diminished dependence on intracellular oxygen levels by integrating a scintillator and a semiconductor as a photosensitizer activated by ionizing radiation. This SZNP agent is the first example of using a scintillator in X-ray radiation downconversion to match the energy gap of a semiconductor to generate ROS from water molecules for efficient radiation-induced type I PDT. The method demonstrates substantially enhanced antitumor therapeutic efficacy with minimized dependencies on the depth and oxygen levels both in vitro and in vivo. Alternative PDT agents with designs as required may be constructed which employ various combinations of scintillators and semiconductors. Despite promising potential for clinical translation,

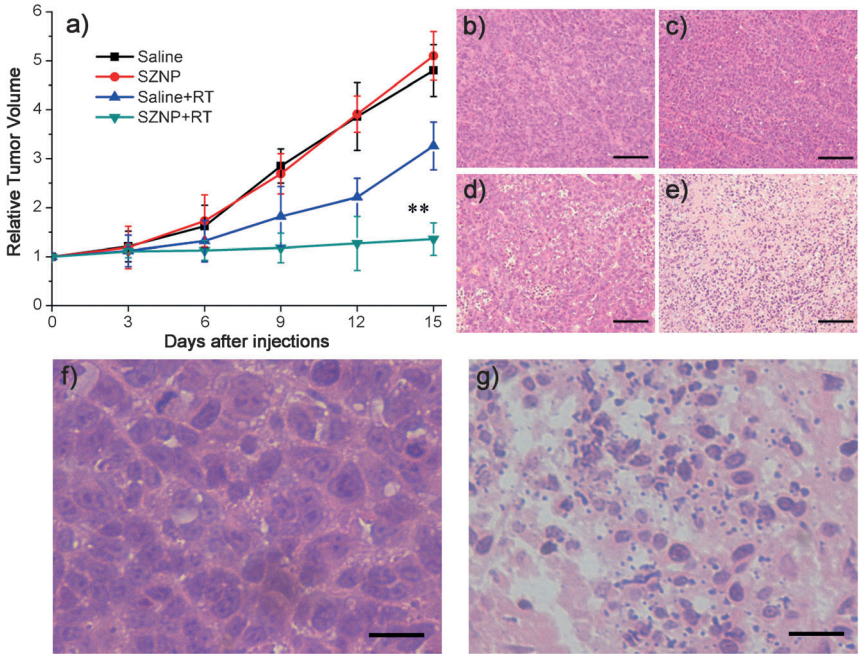

Figure 5. In vivo ionizing-radiation-induced SZNPs-mediated synchronous radiotherapy and PDT. a) The change in relative tumor volume (VV^{-1}_0) with time after exposure of the tissues to different treatments. Data are in mean ± standard errors (6 mice per group), $^{**}P < 0.01$ compared to the control group by using Student's two-tailed t test. H&E staining (hematoxylin and eosin) of tumor tissue sections from mice 48 hours after treatment with b) saline (100 μL), c) SZNPs (1 mg mL^{-1}; 100 μL), d) saline (100 μL) and 8 Gy X-ray radiation, and e) SZNPs (1 mg mL^{-1}; 100 μL) and 8 Gy X-ray radiation. Scale bars in (b–e) = 100 μm. f) and g) are expanded images of (d) and (e), respectively. Scale bars in (f) and (g) = 20 μm.

significant obstacles must be overcome before implementation of these nanoparticles as clinical PDT agents. Solutions to improve the selective accumulation of SZNPs in tumor regions (Figure S11 and S12) and a timely metabolic route should be established. These challenges may be addressed by further modification of the nanoparticle surface and control of its size as required.

Received: August 23, 2014
Revised: November 2, 2014
Published online: December 5, 2014

Keywords: antitumor agents · oxygen · photodynamic therapy · radiotherapy · semiconductors

[1] a) A. E. O'Connor, W. M. Gallagher, A. T. Byrne, *Photochem. Photobiol.* **2009**, *85*, 1053 – 1074; b) B. C. Wilson, M. S. Patterson, *Phys. Med. Biol.* **2008**, *53*, R61 – R109.
[2] J. Fuchs, J. Thiele, *Free Radical Biol. Med.* **1998**, *24*, 835 – 847.
[3] B. W. Henderson, V. H. Fingar, *Cancer Res.* **1987**, *47*, 3110 – 3114.
[4] a) F. Perche, S. Biswas, T. Wang, L. Zhu, V. P. Torchilin, *Angew. Chem. Int. Ed.* **2014**, *53*, 3362 – 3366; *Angew. Chem.* **2014**, *126*, 3430 – 3434; b) P. Vaupel, O. Thews, M. Hoeckel, *Med. Oncol.* **2001**, *18*, 243 – 259.
[5] R. R. Allison, G. H. Downie, R. Cuenca, X.-H. Hu, C. J. H. Childs, C. H. Sibata, *Photodiag. Photodyn. Ther.* **2004**, *1*, 27 – 42.
[6] a) J. Peng, L. Zhao, X. Zhu, Y. Sun, W. Feng, Y. Gao, L. Wang, F. Li, *Biomaterials* **2013**, *34*, 7905 – 7912; b) J. Tian, L. Ding, H. J. Xu, Z. Shen, H. Ju, L. Jia, L. Bao, J. S. Yu, *J. Am. Chem. Soc.* **2013**, *135*, 18850 – 18858; c) N. M. Idris, M. K. Gnanasammandhan, J. Zhang, P. C. Ho, R. Mahendran, Y. Zhang, *Nat. Med.* **2012**, *18*, 1580 – 1585.
[7] a) L. Ma, X. Zou, B. Bui, W. Chen, K. H. Song, T. Solberg, *Appl. Phys. Lett.* **2014**, *105*, 013702; b) L. Ma, X. Zou, W. Chen, *J. Biomed. Nanotechnol.* **2014**, *10*, 1501 – 1508.
[8] A. L. Bulin, C. Truillet, R. Chouikrat, F. Lux, C. Frochot, D. Amans, G. Ledoux, O. Tillement, P. Perriat, M. Barberi-Heyob, C. Dujardin, *J. Phys. Chem. C* **2013**, *117*, 21583 – 21589.
[9] T. S. Mang, T. J. Dougherty, W. R. Potter, D. G. Boyle, S. Somer, J. Moan, *Photochem. Photobiol.* **1987**, *45*, 501 – 506.
[10] a) R. Durand, *In vivo* **1993**, *8*, 691 – 702; b) S. Rockwell, I. T. Dobrucki, E. Y. Kim, S. T. Marrison, V. T. Vu, *Curr. Mol. Med.* **2009**, *9*, 442 – 458.
[11] D. J. Ehrlich, P. F. Moulton, R. M. Osgood, *Opt. Lett.* **1979**, *4*, 184 – 186.
[12] a) H. Zhang, B. Chen, H. Jiang, C. Wang, H. Wang, X. Wang, *Biomaterials* **2011**, *32*, 1906 – 1914; b) Z. Chen, Z. Li, J. Wang, E. Ju, L. Zhou, J. Ren, X. Qu, *Adv. Funct. Mater.* **2014**, *24*, 522 – 529.
[13] Y. Li, W. Zhang, J. Niu, Y. Chen, *Acs Nano* **2012**, *6*, 5164 – 5173.
[14] R. R. Allison, C. H. Sibata, *Photodiag. Photodyn. Ther.* **2010**, *7*, 61 – 75.
[15] A. Y. Satoh, J. E. Trosko, S. J. Masten, *Environ. Sci. Technol.* **2007**, *41*, 2881 – 2887.
[16] C. J. Liu, C. H. Wang, S. T. Chen, H. H. Chen, W. H. Leng, C. C. Chien, C. L. Wang, I. M. Kempson, Y. Hwu, T. C. Lai, M. Hsiao, C. S. Yang, Y. J. Chen, G. Margaritondo, *Phys. Med. Biol.* **2010**, *55*, 931 – 945.
[17] a) S. Anoopkumar-Dukie, T. Conere, G. D. Sisk, A. Allshire, *Br. J. Radiol.* **2009**, *82*, 847 – 854; b) C. Barlow, K. D. Brown, C. X. Deng, D. A. Tagle, A. Wynshaw-Boris, *Nat. Genet.* **1998**, *18*, 298 – 298.
[18] L. B. Harrison, *Oncologist* **2002**, *7*, 492 – 508.
[19] J. Du, J. M. Gebicki, *Int. J. Biochem. Cell Biol.* **2004**, *36*, 2334 – 2343.

